XMM-Newton CCF Release Note

XMM-CAL-SRN-0326

X-ray Loading and Rate-Dependent CTI correction for EPIC-pn Burst Mode

Jan-Uwe Ness, Matteo Guainazzi, Michael Smith

6 March 2015

1 CCF components

Name of CCF	VALDATE	EVALDATE	Blocks changed	XSCS flag
EPN_CTI_0046.CCF	2000-01-01		RATE_DEPENDENT_CTI	NO

This CCF constituent includes an update of the Rate-Dependent CTI (RDCTI) correction for EPIC-pn Burst Mode. This change is required by the implementation of the "X-Ray Loading (XRL)" correction, described in an accompanying CCF Release Note (Ness et al. 2015). The procedure is the same as that described by Guainazzi (2013b).
In 2010, it was discovered that almost all the offset maps taken in scientific filters prior to exposures in EPIC-pn Fast Modes (Burst and Timing) are contaminated by the pointed source (see Guainazzi et al., 2012 for a discussion of this effect). XRL distorts the energy scale in PHA space. This means that the calibration of the RDCTI publicly available so far was based on data, whose energy scale was corrupted in a rate-dependent way. For Timing Mode, this issue has been fixed by first implementing a correction for XRL (XMM-CCF-REL-281, Guainazzi et al. 2014a) and the recalibration of the Rate Dependent CTI correction (Guainazzi 2013b) which was subsequently replaced by the Rate Dependent PHA (RDPHA) correction (Guainazzi 2013a, Guainazzi 2014b, Pintore et al. 2014). The implementation of XRL correction for Burst Mode is described in (Ness et al. 2015) while this release note describes the subsequent RDCTI correction and scientific validation.
As of the 23^{rd} of May 2012, offset maps prior to EPIC-pn exposures in Fast Modes (Burst and Timing) are taken in `CLOSED` filters to avoid XRL in the offset maps. The exposures are thus equivalent to XRL loading corrected observations and the new RDCTI correction is also adequate for these exposures.

2 Description

The principles of the RDCTI calibration for EPIC-pn Timing Modes are described in the original CCF RN (Guainazzi et al. 2009). Readers are referred to this document for a

Number `epproc` run	Description	`withdefaultcal`[a]	`runepreject`	`withxrlcorrection`	`runepfast`
(1)	the status with EPN_CTI_0045.CCF (without XRL correction)	yes	–	–	–
(2)	no energy shift corrections	no	no	no	no
(3)	only the XRL loading correction with parameters $a = 0$ and $b = 1$ using EPN_REJECT_0008.CCF as defined in Ness et al. (2015)	no	yes	yes	no
(4)	XRL plus RDCTI corrections with parameters in the new CCFs EPN_REJECT_0008.CCF and EPN_CTI_0046.CCF	no	yes	yes	yes[b]

[a]Default calibration setting `withrdpha=no`, `withxrlcorrection=yes`, `runepreject=yes`, `runepfast=yes`
[b]Note that `withrdpha=yes` has no effect on Burst Mode data. If `runepfast=yes` is set, then `withrdpha=no` has to be set to avoid that `runepfast` is defaulted to `no` by the SAS.

Table 1: Parameter settings for `epproc`

description of the data reduction and analysis, as well as of the algorithm.
The RDCTI calibration embedded in the new CCF constituent is based on an updated sample of 57 Burst Mode exposures. Out of 102 observations taken until November 2013 with pn Burst Mode exposures, variable sources were excluded, identified by a field integrated light curve exceeding 3 times the standard deviation above or below the average count rate. Eight observations could be time filtered to satisfy this variability criterion by removing time intervals with short flares. Observations whose ODF does not contain an offset map were excluded, because the XRL correction is not reliable in these cases (Guainazzi & Smith 2013).
Four types of events file were produced with the SAS v.14.0.0 task `epproc` with the parameters `withgtiset=yes gtiset=gti.fits burst=yes filterevents=yes` and the varying additional parameters for each run as listed in Table 1.
Source spectra were extracted from each events file, filtering on seven columns `X` with the region expression `box(X,90,0.5,89,0)`, the central column and three columns below and above, respectively. The respective background spectra were extracted with the region expression `(RAWX>=3) && (RAWX<=5) && (RAWY<180)`, scaled to the size of the source region and used in the spectral analysis. All source spectra are featureless in the 1.5–3 keV energy band, and to determine the energy shift, a model was fitted to the 1.5–3 keV energy range of each spectrum (containing the Si and Au edges) using `xspec` with a pure continuum model `tbabs*(diskbb+po)` and a variable gain shift parameter.
For the observation of the supernova remnant Cas A (ObsID 0412180101) the spectrum was extracted from a larger region with the expression `box(X,90,6,89,0)` because it is an extended source. Further, the spectrum of Cas A is not featureless, and the model `tbabs*(vapec+vapec)` was used to determine a gain shift.
The results for the four events files listed in Table 1 are illustrated in Fig. 1. The bottom

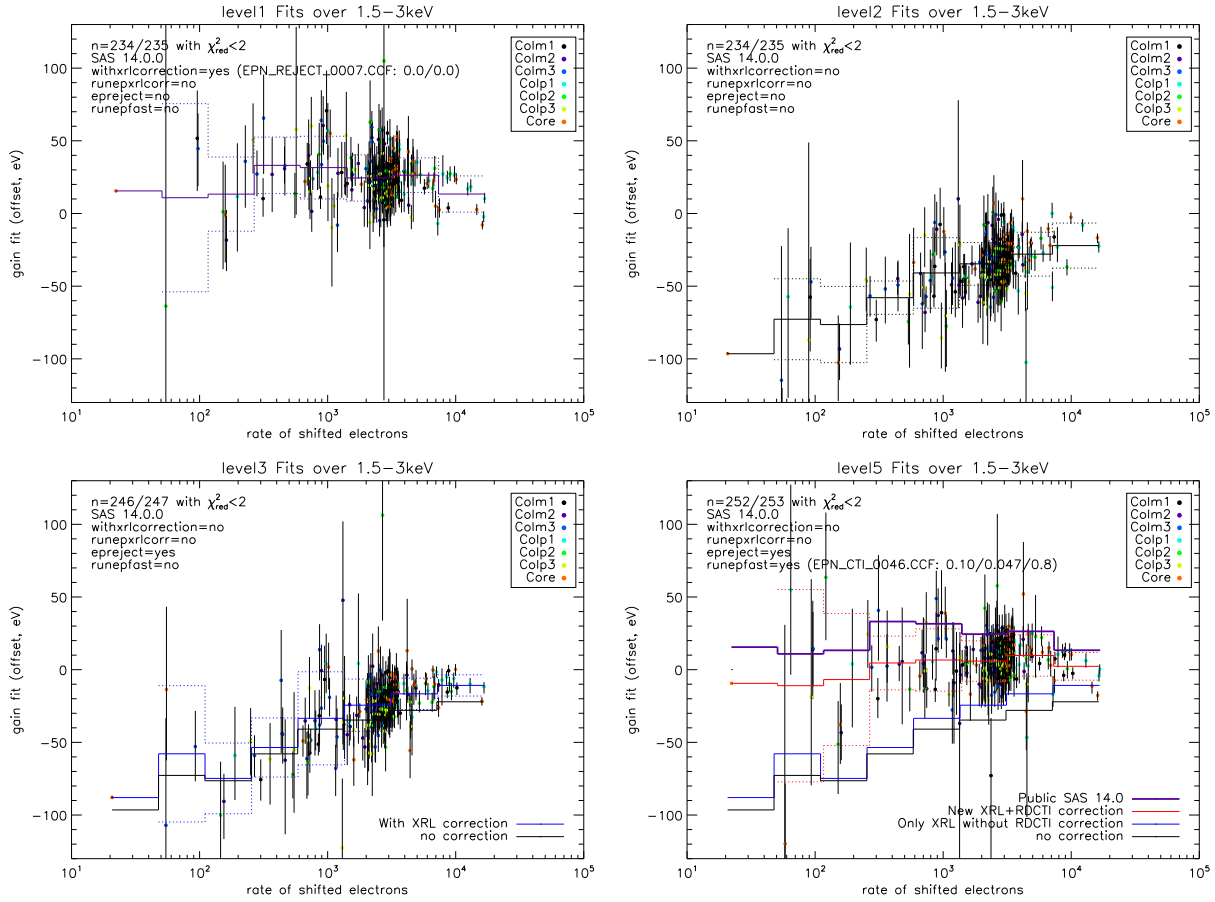

Figure 1: Rate of shifted electrons versus best-fit gain, in eV, determined from model fitting to the spectra obtained from the events files reduced using SAS 14.0.0 with the CCF file EPN_CTI_0045.CCF (top left), no energy shift corrections (top right), XRL correction (bottom left), and XRL+RDCTI correction (bottom right), using the corresponding `epproc` parameters given in Table 1 and EPN_CTI_0046.CCF. The histograms are average gain shifts over the corresponding range of rates of electron shift, where the dotted histograms indicate the spread in terms of standard deviation within each bin. In the bottom panels, the blue histograms indicate the non-corrected curve from the top right panel, and in the bottom right panel, the purple histogram shows the results from the public SAS. The improvement from the public SAS to the new XRL+RDCTI correction can clearly be seen as the residual gain shifts have been systematically reduced."

left panel demonstrates that the XRL loading correction described in the accompanying CCF release note Ness et al. (2015) is much smaller than the RDCTI correction that is shown in the bottom right panel. Comparison of the purple and red histograms in the bottom right panel, i.e., results with current public CCF and results with new XRL+RDCTI corrections, demonstrates that the new corrections are better than the currently public CCF.

To compute the new RDCTI used EPN_CTI_0046.CCF, the data points in the bottom left panel, thus after XRL correction, are used to compute new parameters a_0, a_1, and a_2 in the calibration relation $G = a_0(N_e)^{a_1} + a_2$, where G is the gain factor (calculated around the Si and Au instrumental edges, *i.e.* around 2 keV), N_e is the rate of shifted

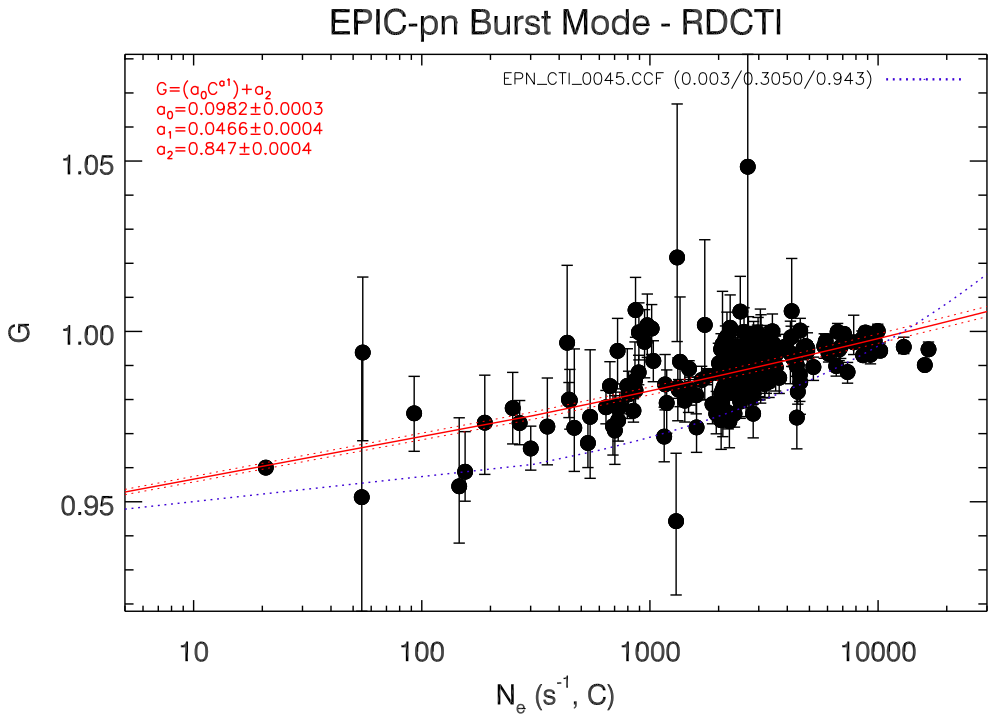

Figure 2: RDCTI calibration curve in the new version, `EPN_CTI_0046.CCF`. The *solid red line* represents the best-fit function corresponding to the parameters given in the top left. The *red dotted lines* represent the envelope of the same function corresponding to the 1σ error on the best-fit parameters. For comparison, the calibration curve from `EPN_CTI_0045.CCF` is included with the blue dotted line.

a_0	a_1	a_2
0.00982 ± 0.0003	0.0466 ± 0.004	0.847 ± 0.0004

Table 2: Parameters of the RDCTI calibration function (and 1σ statistical uncertainties) in `EPN_CTI_0029.CCF`

electrons, and a_i are fit parameters. The gain factor G is calculated by the SAS using the parameters a_i as given in the extension `RATE_DEPENDENT_CTI` of the CCF component `EPN_CTI_0046.CCF`.

The RDCTI calibration curve is shown in Fig. 2, where the black filled circles are gain factors

normalized to 2200 from the bottom right panel of Fig 1, the red curve is the best fit with parameters and errors given in the left legend, the dotted red lines are the uncertainty ranges, and the blue dotted line is the calibration curve in the current public CCF, version 45, leading to the data points in the top left panel of Fig. 1. The final parameters are listed in Tab. 2. The CCF contains only the best-fit, thus the errors are not used to calculate the correction to the energy scale.

3 Scientific Impact of this Update

Together with the associated calibration of the XRL correction (Ness et al. 2015), the update of the RDCTI calibration is intended to provide a full recalibration of the energy scale in EPIC-pn Burst Mode.

4 Estimated Scientific Quality

Doubts have been expressed on the accuracy of the energy-dependence of the RDCTI in burst mode (Walton et al. 2012). As this correction is calibrated at $\simeq$2 keV, a wrong energy-dependence could yield significant errors at other energies such as the iron line energies. Since the true origin of the RDCTI is unknown, the calibration relation is purely empirical, and the performance of the new calibration needs to be verified at other energies.

In Fig. 3, we show the spectra of two of the four observations of 4U1700-37 from the events files (1), (2), and (4) in Table 1, where the spectrum from (3) is not shown because these observations contain no offset map. The top plot, ObsID 0083280201, is used to check the performance at softer energies, and one can see that all three spectra are similar, thus the correction has no important effect. Meanwhile, in the 5–8 keV range where the Fe transitions arise, significant energy shifts are encountered with different corrections. The model, shown in black, contains no Fe lines which will then show up as emission features in the residual plots shown in the respective bottom panels. For ObsID 0083280401, the Fe I absorption edge at 7.11 keV (Kallman et al. 2004) can be seen to agree best with EPN_CTI_0046.CCF calibration while EPN_CTI_0045.CCF overcorrects the energies. Also the unresolved Fe I Kα_1 and Kα_2 fluorescent lines at 6.403/6.390 keV are at the expected energy with the new calibration while overcorrected by $\sim$ 100 eV with the currently public CCF.

As an example of a low count rate spectrum, we used ObsID 0412180101 of Cas A and extended source with a count rate of 340 counts per second, and rate of shifted electrons of 22.26 s^{-1}. In addition to the Burst Mode observation, there are observations in Full Frame and Large Window Modes available for comparison. As a reference we have used an observation in Large Window Mode (ObsID 0110011801) which completely covers the full remnant. The reference spectrum was extracted from a circle centered at RA=23:23:29.679, DEC=+58:48:54.10 with a radius of 190 arcseconds. The comparison is illustrated in Fig. 4 from which we conclude that the energy scale at the Fe line energies is slightly inferior in the new calibration compared to the presently public version EPN_CTI_0045.CCF SAS. We point out, however, that at the count rate regime of Cas A, observers will most likely not use the Burst Mode. Although users should be aware of the small loss in calibration quality in the low count rate regime, the calibration is optimised for the much larger number of high count rate observations, where the improvements obtained with the new calibration are substantial.

Finally, we study the Fe absorption lines in GRO J1655-40 with Fig. 5. They can only

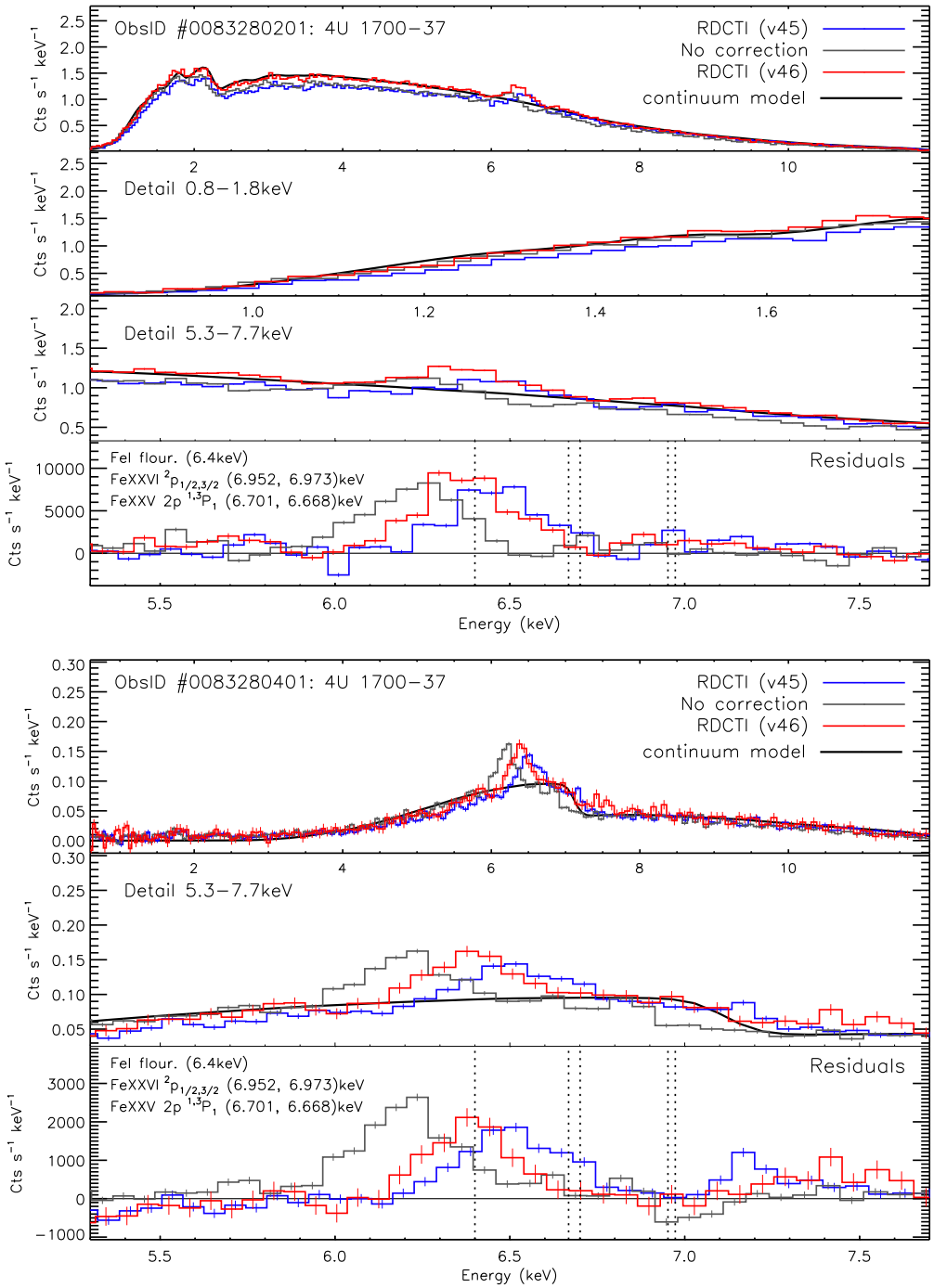

Figure 3: Comparison of two spectra of 4U1700-37 using the public CCF, thus EPN_CTI_0045.CCF and no XRL correction, in SAS 14.0.0 (extraction (1) in Table 1 in blue), without energy shift corrections (2, grey), and with the RDCTI correction using EPN_CTI_0046.CCF (4, red). No XRL correction could be applied because there is no offset map in these observations. In ObsID 0083280201, a strong soft component was present which is similar in all extractions. The bottom panel shows the residual between observations and model, and the Fe line can be seen to best be centered around the Fe I fluorescence line at 6.4 keV with the CCF file EPN_CTI_0046.CCF. ObsID 0083280401 contains much more prominent Fe line emission as well as the Fe edge at 7.11 keV which is also best reproduced with the new calibration (red, see also middle panel of bottom plot).

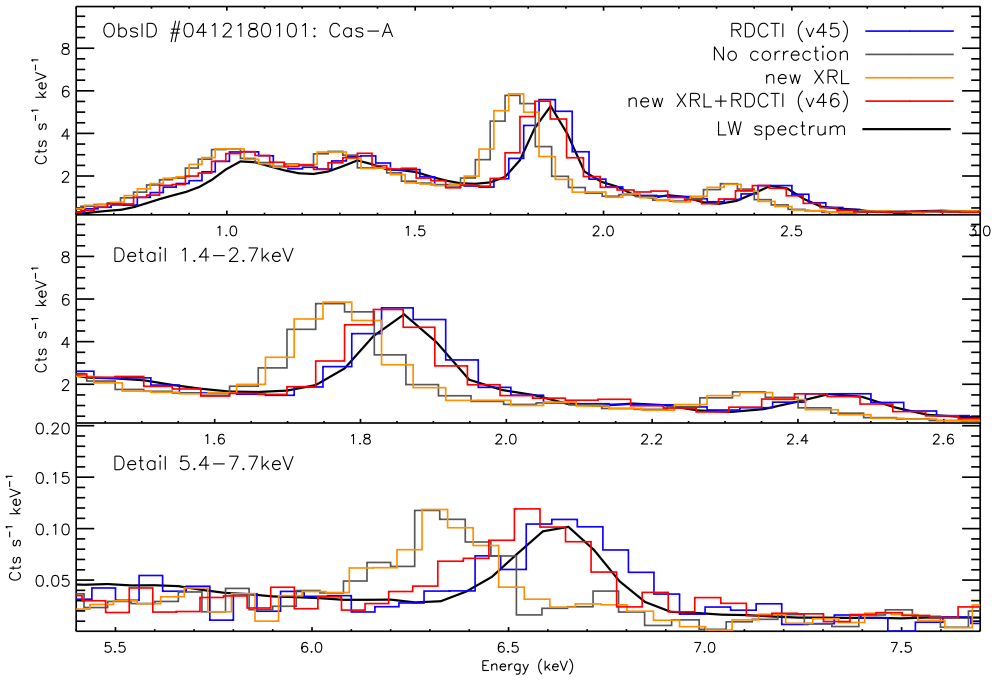

Figure 4: Same comparison as Fig. 3 for Cas A for which an offset map is available, and the spectrum extracted from an events file only corrected for XRL is included with the orange line (run #3 in Table 1). The performance of the energy scale calibration can be gauged from emission lines that are assumed to be measured at their correct energies in an observation taken in Large Window Mode, shown in black. While at soft energies, the energy scale is hardly affected by any correction, the new calibration at 6.5 keV is slightly inferiour compared to EPN_CTI_0045.CCF.

be seen in the residual plot in the bottom. The differences in energy scale are very small yielding a slight advantage with the new calibration parameters.

5 Expected updates

Guainazzi (2013a) describes another algorithm to correct for the intrinsic rate-dependence of the energy scale: the Rate-Dependent PHA correction (RDPHA). It acts on the spectra in `PHA`, and it is thus independent on any astrophysical assumptions. This algorithm is already the default for the Timing Mode and at the time of writing, studies are ongoing to also implement it for the Burst Mode. In the meantime, the RDCTI correction has been updated, not to delay unnecessarily the public delivery of an energy scale correction consistent with the XRL correction.

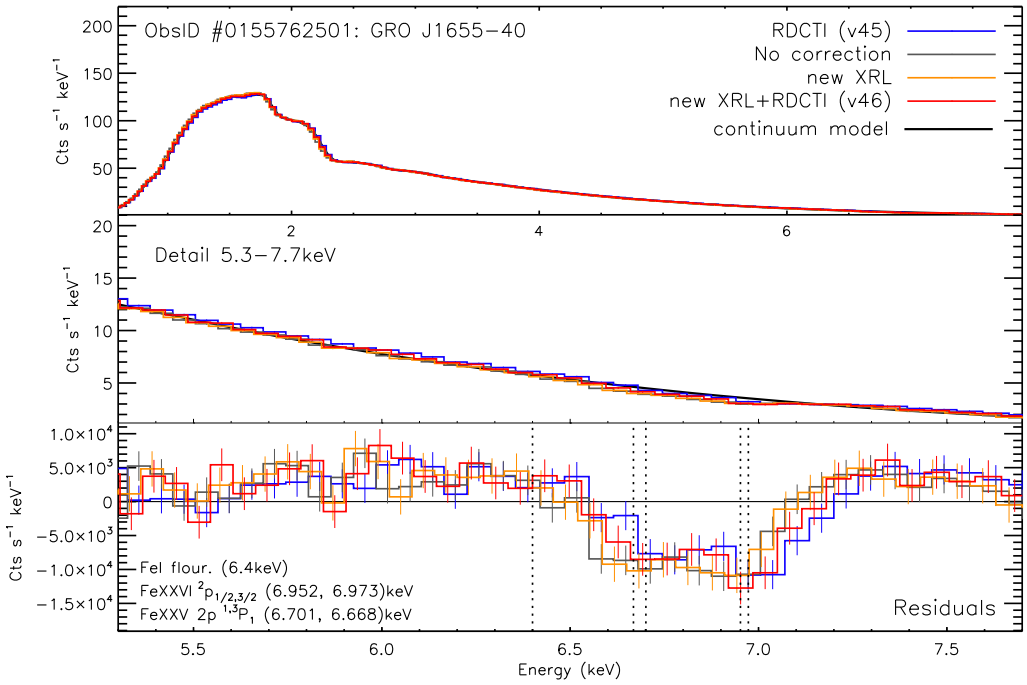

Figure 5: Same as Fig. 4 for GRO J1655-40, using a continuum model as reference in black. The Fe lines are seen in absorption with slightly better calibration with the XRL+RDCTI parameters using the new calibration files EPN_REJECT_0008.CCF and EPN_CTI_0046.CCF.

6 References

Guainazzi M. et al. 2009, XMM-CCF-REL-256,
"Rate-dependent CTI correction for EPIC-pn Timing Modes: SASv9.0 update"
(available at: `http://xmm2.esac.esa.int/docs/documents/CAL-SRN-0256-1-0.ps.gz`)

Guainazzi M., et al. 2012, XMM-CCF-REL-0281,
"Support to the X-ray Loading correction in EPIC-pn Fast Modes"
(available at: `http://xmm2.esac.esa.int/docs/documents/CAL-SRN-0281-1-0.pdf`)

Guainazzi M. 2013a, XMM-CCF-REL-0299,
"Coefficients of the Rate-Dependent PHA (RDPHA) correction based on the derivative spectra"
(available at: `http://xmm2.esac.esa.int/docs/documents/CAL-SRN-0299-1-1.ps.gz`)

Guainazzi M. 2013b, XMM-CCF-REL-0304,
"Post-XRL Rate-Dependent CTI correction for EPIC-pn Timing Mode"
(available at: `http://xmm2.esac.esa.int/docs/.../CAL-SRN-0312-1-4.pdf`)

Guainazzi M., et al. 2014a, XMM-SOC-CAL-TN-0083,
"Spectral calibration accuracy in EPIC-pn fast modes"
(available at: `http://xmm2.esac.esa.int/docs/documents/CAL-TN-0083.pdf`)

Guainazzi M. 2014b, XMM-CCF-REL-0312,
"RDPHA calibration in the Fe line regime for EPIC-pn Timing Mode"
(available at: `http://xmm2.esac.esa.int/docs/documents/CAL-SRN-0312-1-1.pdf`)

Kallman, T., et al. 2004, ApJS 155, 675,
"Photoionization Modeling and the K Lines of Iron"

Ness, J.U., Guainazzi M. and Smith M. 2015, XMM-CCF-REL-0325,
"X-ray Loading correction for EPIC-pn Burst Mode"
(available at: `http://xmm2.esac.esa.int/docs/documents/CAL-SRN-0325-1-1.pdf`)

Pintore, F. et al. 2014, MNRAS 445, 3745
"Testing rate-dependent corrections on timing mode EPIC-pn spectra of the accreting neutron star GX 13+1"

Walton D., et al. 2012, MNRAS, 422, 2510
The similarity of broad iron lines in X-ray binaries and active galactic nuclei